CrossMark

Study on dielectric, optic and magnetic properties of manganese and nickel co-doped bismuth ferrite thin film

K. T. Liu[1] · J. Li[1] · J. B. Xu[2] · F. L. Xu[2,3] · L. Wang[2,3] · L. Bian[2]

Abstract $BiFeO_3$ (BFO), Mn (7.5%)-doped BFO (BFMO), Ni (7.5%)-doped BFO (BFNO), as well as Mn (3.75%) and Ni (3.75%) co-doped BFO (BFMNO) films were deposited on indium tin oxide (ITO)/glass substrates by sol–gel process. X-ray diffraction (XRD) analysis indicated that the BFO and BFNO presented single rhombohedral structure, while BFMO and BFMNO thin films presented tetragonal structure. The current density versus electric field (*J–E*) characteristics indicated that leakage conduction can be decreased with Mn and/or Ni doped. The films conduction mechanism of BFO and BFNO are space-charge-limited current in the high electric field region, while for BFMO and BFMNO is Ohmic's conduction in all electric field region. The optical band gap of the BFO, BFMO, BFNO and BFMNO thin films are 2.18, 2.22, 2.3 and 2.32 eV, respectively. The inhomogeneous spin-modulated magnetic structure of BiFeO3 was modified by Mn and/or Ni substitution.

1 Introduction

Recently, multiferroic BFO has attracted enormous attention due to its potential applications in advanced data storage devices, spin valve, spintronics and sensors [1–4]. Meanwhile, BFO also is regard as a kind of photocatalytic or photovoltaic material and has been studied extensively because of possessing a relatively narrow band gap [5, 6]. The thin films of BFO has drawn people more and more attention because of its excellent physical properties such as spontaneous polarization [1], saturation magnetization [7], and a piezoelectric response [8], which are significantly enhanced relative to that of the bulk [9].

However, low-resistivity of BFO thin films still is a major problem for its potential practical application. The mechanism inducing resistivity in BFO films can be attributed to the variable oxidation states of Fe ions (Fe^{3+} to Fe^{2+}), which requires oxygen vacancies (V_o^{2+}) for charge compensation and produces electron hopping in films [10]. Another mechanism is due to high volatility of atom Bi and generates V_{Bi}^{3-} in lattice accompanied by the emergence of the second-phase (such as $Bi_2Fe_4O_9$) [11]. In order to solve the low-resistivity problem, the site-engineering concept in Bi-site or Fe-site has been proposed to control volatility of Bi atom and suppress generation of oxygen vacancies. Gao et al. prepared Dy-doped BFO on Pt/Ti/SiO$_2$/Si (100) substrates via chemistry solution deposition [12]; T. Kawae et al. fabricated Mn and Ti co-doped BFO on Pt/SrTiO$_3$ by pulse laser deposition [13], the both analyzed electric properties and found electric properties of BFO enhanced.

In the case of preparation of BFO thin films by sol–gel process, the crystallization temperature is lower than 550 °C for avoiding the formation of interface layer between thin film and substrate. On the other hand, the volatility temperature of Bi atom is higher than 700 °C presented during the experiment. For this reason, we thought the variable valences of Fe atom should play more important role in inducing resistivity of BFO thin films, rather than volatility of atom Bi.

✉ J. Li
xjlijin@163.com

1 College of Physics Science and Technology, Xinjiang University, Urumqi 830046, Xinjiang, China

2 Xinjiang Key Laboratory of Electronic Information Materials and Devices, Xinjiang Technical Institute of Physics and Chemistry, Chinese Academy of Sciences, Urumqi 830011, China

3 Graduate University of Chinese Academy of Sciences, Beijing 100049, China

In this paper, we attempt to further improve the resistivity of BFO thin films by Mn^{2+} and/or Ni^{2+} doping. Mn and/Ni-doped BFO thin films were prepared on indium tin oxide (ITO)/Glass substrate. ITO layer is semiconductor-like transparent thin film which can be used to as electrode to investigate the optical property of the thin films. The structural phase transition, resistivity, dielectric, optical and magnetic properties of Mn and/or-doped BFO thin films were discussed in detail.

2 Experimental procedure

Pure $BiFeO_3$ (BFO), Mn (7.5%)-doped BFO (BFMO), Ni (7.5%)-doped BFO (BFNO), as well as Mn (3.75%) and Ni (3.75%) co-doped BFO (BFMNO) thin films were prepared on ITO/Glass substrates by a conventional sol–gel process. The bismuth nitrate $Bi(NO_3)_3 \cdot 5H_2O$, iron nitrate $Fe(NO_3)_3 \cdot 9H_2O$, manganese acetate $(C_4H_6MnO_4 \cdot 4H_2O)$ and nickelous acetate $(C_4H_6NiO_4 \cdot 4H_2O)$ were mixed in citric acid under constant stirring at $80\,°C$ for 30 min according to the metal ion ratios and then 2-methoxyethanol was added under constant stirring for 180 min at room temperature. The depositions were carried out by spin coating at 3000 rpm for 20 s. The wet films were pre-annealed at $350\,°C$ for 5 min and, followed by an annealing at $550\,°C$ in air for 30 min. The above procedures were repeated several times to obtain the desired thickness. The structure of poly-BFO films was confirmed by checking the X-ray diffraction data (XRD) (Bruker D8). The surface morphologies were detected by using an atomic force microscope (NT-MDT Solver P47). The cross sectional images were measured by using scanning electric microscope (SEM) (Hitachi SU9000). The dielectric properties of the thin films were measured by an impedance analyzer (E4980A Agilent Inc). Their leakage current behavior was characterized by a Keithley 2410 m. The optical properties were measured by UV–vis (Shimadzu UV 2501). The magnetic hysteresis (M–H) loops were collected using a vibrating sample magnetometer (VSM) (Lake Shore 7410).

3 Result and discussion

The XRD peaks of all films shown in Fig. 1a match well to those of the polycrystalline perovskite structure with no impurity phases. Note that BFO and BFNO films showed similar distorted rhombohedral $R3c$ structure with strong diffraction peaks of (012), (104) and (110). But the intensity of these three diffraction peaks for BFNO was weaker than BFO, indicating that the crystallite size of BFNO was smaller than BFO [14]. Figure 1b displays the magnified version of the XRD patterns in the 2θ range of 31°–33°, which reveals an evolution of the (104) and (110) diffraction peaks in BFMO and BFMNO. This phenomenon indicates that substitution induces structural distortion. It shows BFMO and BFMNO films exhibited the similar orthorhombic or tetragonal structure, which shows that Mn^{3+} cation may play an important role in lattice structure transforming [15]. The (110) diffraction peak is the strongest one in BFMO while the (012) is the strongest one in BFMNO, which may be attributed to Ni^{3+} cation having the closer ionic radius to Fe^{3+} cation, comparing to the Mn^{3+} cation

Fig. 1 **a** XRD patterns of BFO, BFMO, BFNO and BFMNO films at room temperature. **b** Magnified view of the diffraction peaks (104) and (110)
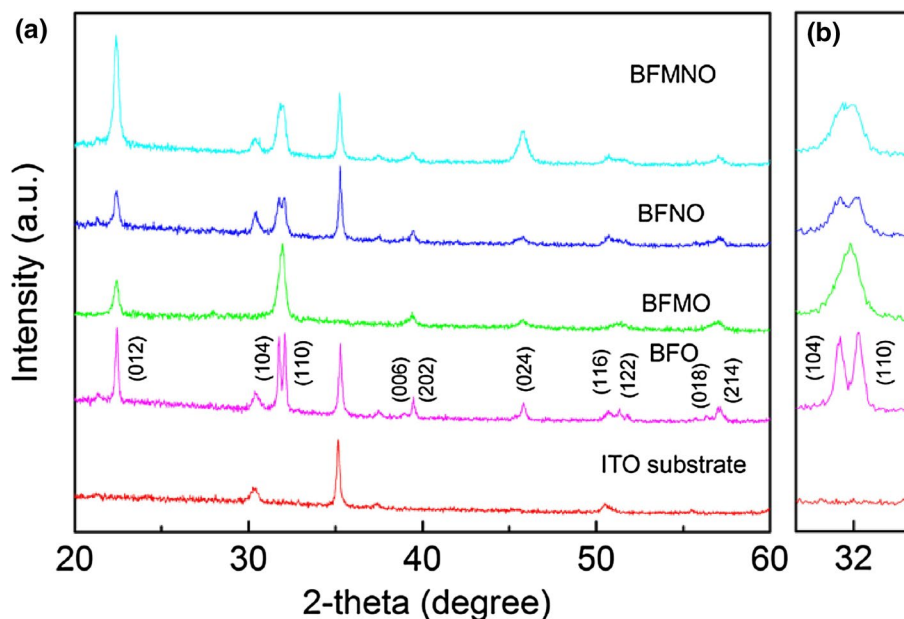
[16]. These differences of structure can induce to the different properties.

Figure 2a–d showed surface AFM images of thin films. It can be seen that the crystallite size of BFMO, BFNO and BFMNO films were much smaller than pure BFO. This is because that the manganese acetate and nickelous acetate decomposed to manganese oxide and nikelous oxide at the pyrolysis procedure, which can act as heterogeneous nucleation sites in perovskite phase [17]. Figure 2e was the cross-sectional of BFO, which showed the thickness of the film was about 300 nm.

Figure 3a showed current density vs electric field (J–E) characteristics of BFO, BFMO, BFNO and BFMNO film capacitors on ITO/glass measured at RT. It can be clearly seen that the leakage current densities of doped BFO thin films were lower than pure BFO. In pure BFO, the reduction in Fe^{3+} species to Fe^{2+} creates oxygen vacancies for charge compensation and in turn it increases the conductivity [18]. The Mn^{2+} and /or Ni^{2+} can compensate for the charges generated from the oxygen vacancies with the appropriate amount of charge balance to lower the leakage current [19].

Figure 3b shows the log I vs log V plots of BFO, BFMO, BFNO and BFMNO. At the low electric field, the exponentials of $a = 1.0$ and 1.1 for BFO and BFNO films respectively, which indicates that BFO and BFNO films are subject to Ohm's law. Whereas the leakage current increases rapidly with the exponentials of $a = 1.9$ and 4.4 for BFO and BFNO films respectively as increasing the electric field, indicating that the two films are subject to space charge limited conduction (SCLC) mechanism. This phenomenon can be explained by Lampert's triangle [20], in

Fig. 2 AFM images of **a** BFO, **b** BFMO, **c** BFNO and **d** BFMNO films on ITO/glass substrates. **e** Cross-sectional SEM images of the BFO films
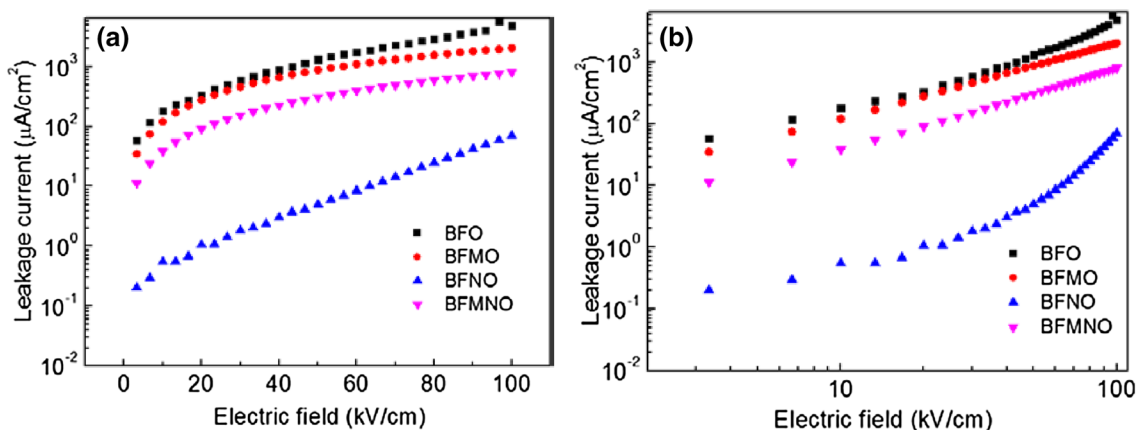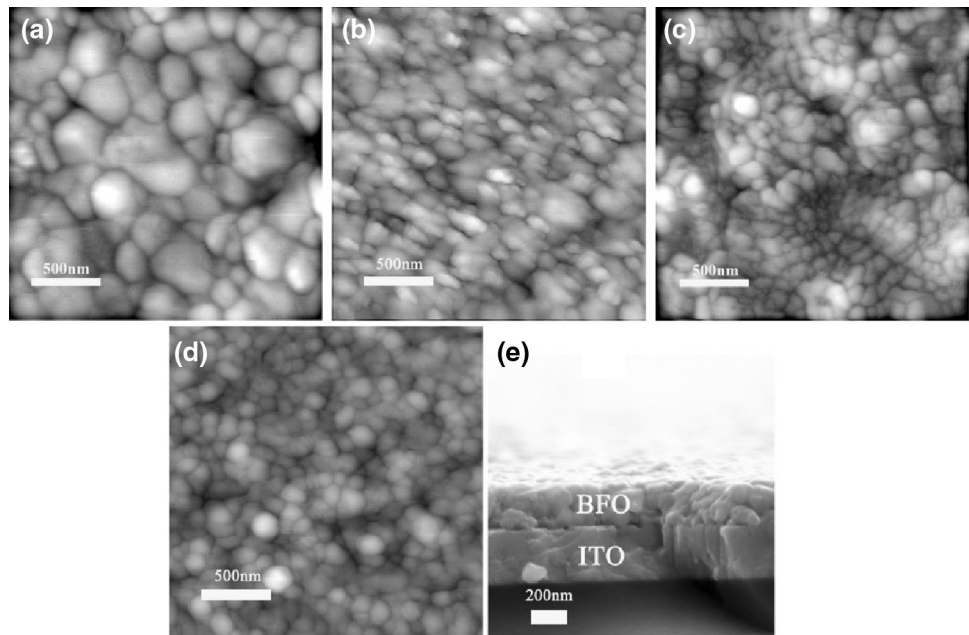

Fig. 3 J–E characteristics of BFO, BFMO, BFNO and BFMNO films on ITO/glass substrates measured at RT. **a** Semilogarithmic and **b** logarithmic plots

the insulators with traps, there are two types mechanism in different electric fields: Ohm's law and SCLC. At a low applied electric field, the injected electrons from the cathode can be swiftly transported via the conduction band, resulting in a drift current. More electrons are injected into the insulator with the increase of electric field, giving rise to the unbalance of space charges, thus the SCLC becomes to dominate [21].

In case of BFMO and BFMNO films, the leakage current mechanism was found to be only subject to Ohm's law with the exponentials of $a = 1.21$ and 1.29 for BFMO and BFMNO film, respectively. The leakage current conduction mechanism of BFO has no changes with Ni doping, while Mn doped and Mn and Ni co-doped change the leakage current conduction mechanism. These may be caused by the transformation of lattice structure. Although BFMO and BFMNO have the same leakage mechanism, the exponential of BFMNO is a little larger than BFMO, which indicates the Ni element can also affect the leakage mechanism.

In order to study the dielectric properties, the complex dielectric constant $\varepsilon^* = \varepsilon' - i\varepsilon''$ (ε': real part; ε'': imaginary part) was measured at room temperature in the range of 100 Hz–2 MHz. Figure 4a showed the frequency spectrum curves. It showed the dielectric constant ε' of BFMO and BFNO were smaller than BFO, while the dielectric constant of BFMNO was bigger than BFO. The dielectric constant ε' BFO and BFNO both decreased rapidly in the high frequency range (100 Hz–2 MHz) and dielectric constant ε'' presented a peak value at 200 kHz and 1.5 MHz respectively. It indicates BFO and BFNO are both order–disorder ferroelectric whose main characteristic is that dielectric polarization is equivalent to orientation polarization of dipoles [22]. But the relaxation frequency of BFNO is larger than BFO, according to the Debye

dielectric relaxation, ε'' take the maximum value at $\omega\tau = 1$, so the relaxation time of BFNO is smaller than BFO. It implies that BFNO present more uniform alignment of dipoles [23]. While the dielectric constant ε' of BFMO and BFMNO don't decrease largely in this measure frequency range and the dielectric constant ε'' don't present a peak value. The resonance frequency of BFMO and BFMNO may be above the 2 MHz, so this high relaxation frequency indicates that the dielectric polarization mainly comes from the displacement polarization of dipoles. It can be confirmed that BFMO and BFMNO are displacement ferroelectric whose main feature is ultra-high dielectric relaxation frequency [24]. Ni doped doesn't change the type of ferroelectric, while Mn doped and Mn, Ni co-doped change the type of ferroelectric. These results can be explained by the transformation of lattice structure, the lattice structure don't have any changes with only Ni doped, while Mn doped and Mn, Ni co-doped lead to the transformation of lattice structure. Figure 4b shows the frequency dependence of dielectric loss. It can be found that the dielectric loss decreases largely in the high frequency range with Mn and/or Ni doped, which may be the reason to leakage current decreased [25].

Optic band gap is an important parameter for photovoltaic materials. The ultraviolet–visible absorption spectrum date of BFO, BFMO, BFNO and BFMNO were measured in this paper, and the optic band gap can be calculated via Tauc equation shown below [26].

$$\alpha hv = A(hv - E_g)^{n/2} \tag{1}$$

where α is absorption coefficient, A is a constant, hv is the photon energy, Eg is the energy band gap, n is determined by the energy band structure of electron, $n = 1$
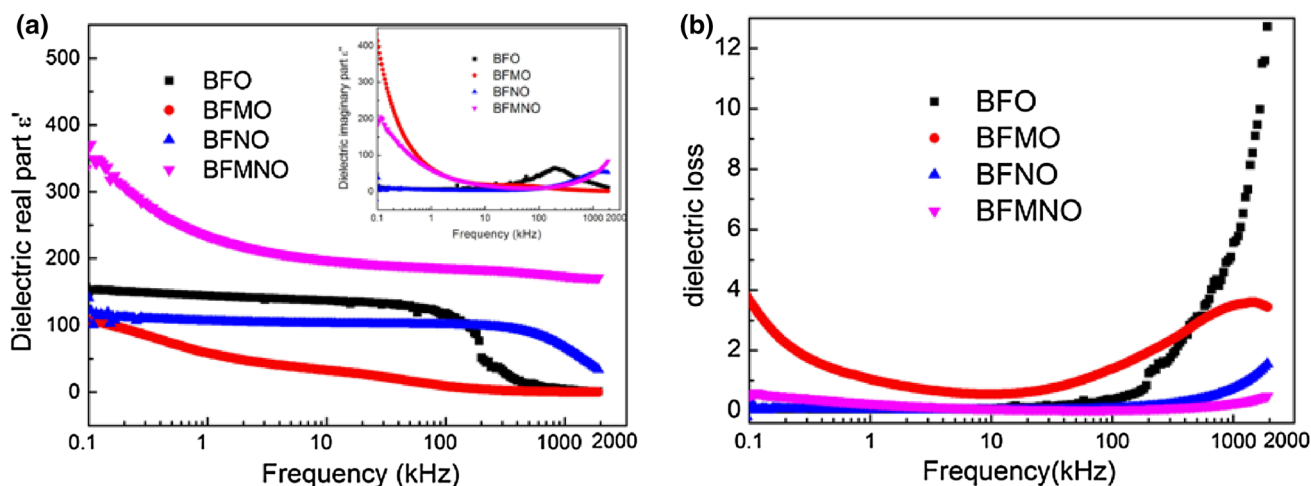

Fig. 4 **a** Frequency dependence of dielectric real part ε' for the samples measured at 30 °C, *inset* shows frequency dependence of dielectric imaginary part ε''. **b** Frequency dependence of the dielectric constant and dielectric loss of the samples

for direct band gap and 4 for indirect band gap. Figure 5 shows the $(\alpha h\nu)^2 - (h\nu)$ plots of BFO, BFMO, BFNO and BFMNO. Extrapolation of linear region of these plots to $(\alpha h\nu)^2 = 0$ gives corresponding direct energy band gap. It shows that the band gap of BFO, BFMO, BFNO and BFMNO are 2.18, 2.22, 2.3 and 2.32 eV, respectively. These values are consistent to report of Gao et al. [5]. There are two main factors leading to broaden the band gap: one is the lattice parameter becomes smaller [27]; another is the carrier concentration in materials becomes less [21]. In this paper, the cationic radius of Mn^{3+} (r = 0.058 nm) and Ni^{3+} (r = 0.056 nm) both are larger than Fe^{3+} (r = 0.055 nm), and the lattice parameter would become larger when Mn and/or Ni doped. So the main factor to result in broadening the band gap is the carrier concentration in materials becomes less, according to the Boltzmann equation [28]:

$$n_i = p_i = \sqrt{N_c N_v} \times \exp\left(-\frac{E_g}{2k_B T}\right) \qquad (2)$$

where n_i and p_i are the intrinsic density of electron and hole respectively, N_c is the density of states (DOS) at bottom of conduction band, N_v is the DOS at the top of valence band, E_g is the energy band gap, k is the Boltzmann constant, and T is the absolute temperature. From the leakage current part discussed above, the leakage current and oxygen vacancies concentration of BFO decrease after Mn and/or Ni doped, and therefore lead to the increase of band gap.

Figure 6 shows the M–H curves of BFO, BFMO, BFNO and BFMNO thin films. The curve of pure BFO is almost a line, which manifests that pure BFO don't present room temperature ferromagnetism. While Mn and/or Ni doped BFO all can get a weak ferromagnetic hysteresis loops at room temperature and have larger magnetization, indicating that they all present room temperature ferromagnetism. The BFMO is well-saturated at about 2000 Oe. BFNO and BFMNO are not well-saturated in this measuring range, but BFMNO tends to be more saturated than BFNO. The amplification of center region is
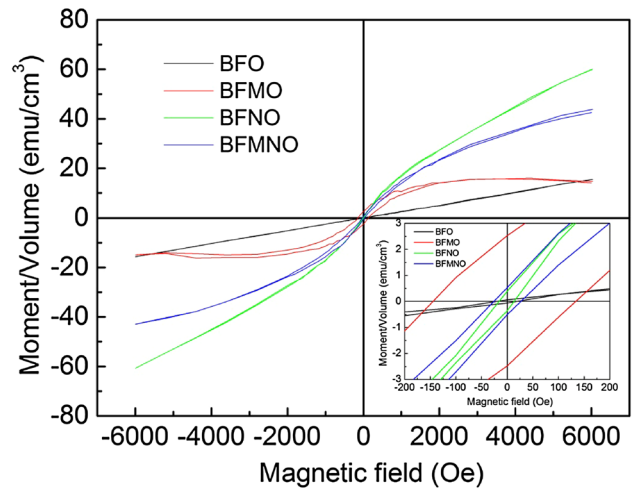

Fig. 6 M–H *curvess* of BFM, BFMO, BFNO and BFMNO

Fig. 5 Plot of $(\alpha h\nu)^2$ vs photon energy $(h\nu)$ for BFO, BFMO, BFNO and BFMNO

shown inset of Fig. 6. The residual magnetization and coercive field of BFO, BFMO, BFNO and BFMNO are about 0.06 emu/cm^3 and 20 Oe, 2.5 emu/cm^3 and 130 Oe, 0.4 emu/cm^3 and 18 Oe, 0.5 emu/cm^3 and 23 Oe respectively. In fact, BFO is known to be antiferromagnetic having a G-type magnetic structure [29], but has a residual magnetic moment due to a canted spin structure (weak ferromagnetic) [30].

It can be seen that doped BFO have higher residual magnetization and coercive field than pure BFO [16, 31]. BFMO has higher remanent magnetization and coercive field compared with other samples. The ferromagnetism of BFO is enhanced with Mn and/or Ni doped. Mn^{2+} and/or Ni^{2+} doped can lead to make the lattice structure transformed as the radius of Mn^{2+} and Ni^{2+} are bigger than Fe^{3+}, therefore destroy the original spin cycloid and form the homogeneous spin structure. The lattice transformation makes the potential magnetism released and result in observed room temperature ferromagnetism. But the effect of Mn and Ni to BFO is different because they affect the structure differently.

4 Conclusions

In conclusion, BFO, BFMO, BFNO, and BFMNO films were fabricated on indium tin oxide (ITO)/glass substrates by sol–gel process. BFO and BFNO presented single rhombohedral, while BFMO and BFMNO thin films presented tetragonal structure. Leakage current conduction can be decreased with Mn and/or Ni doped. The conduction mechanism of BFO and BFNO are space-charge-limited current in the high electric field region, as well as BFMO and BFMNO are Ohmic's conduction in whole electric field region. The optical band gap of the BFO, BFMO, BFNO and BFMNO thin films are 2.18, 2.22, 2.3 and 2.32 eV, respectively. The inhomogeneous spin-modulated magnetic structure of BFO was modified by Mn and/or Ni substitution and ferromagnetism was enhanced.

References

1. J. Wang, J.B. Neaton, H. Zheng, V. Nagarajan, S.B. Ogale, B. Liu, D. Viehland, V. Vaithyanathan, D.G. Schlom, U.V. Waghmare, N.A. Spaldin, K.M. Rabe, M. Wuttig, R. Ramesh, Science **299**, 1719 (2003)
2. J.B. Neaton, C. Ederer, U.V. Waghmare, N.A. Spaldin, K.M. Rabe, Phys. Rev. B **71**, 014113 (2005)
3. T. Zhao, A. Scholl, F. Zavaliche, K. Lee, M. Barry, A. Doran, M.P. Cruz, Y.H. Chu, C. Ederer, N.A. Spaldin, R.R. Das, D.M. Kim, S.H. Baek, C.B. Eom, R. Ramesh, Nat. Mater. **5**, 823 (2006)
4. Y.H. Chu, L.W. Martin, M.B. Holcomb, M. Gajek, S.J. Han, Q. He, N. Balke, C.H. Yang, D. Lee, W. Hu, Q. Zhan, P.L. Yang, A. Fraile-Rodriguez, A. Scholl, S.X. Wang, R. Ramesh, Nat. Mater. **7**, 478 (2008)
5. F. Gao, X. Chen, K. Yin, S.Z. Ren, F. Yuan, T. Yu, Z. Zou, J.M. Liu, Adv. Mater. **19**, 2889 (2007)
6. T. Choi, S. Lee, Y.J. Choi, V. Kiryukhin, S.W. Cheong, Science **324**, 63 (2009)
7. K.Y. Yun, M. Noda, M. Okuyama, H. Saeki, H. Tabata, K. Saito, J. Appl. Phys. **96**, 3399 (2004)
8. R.J. Zeches, M.D. Rossell, J.X. Zhang, A.J. Hatt, Q. He, C.H. Yang, A. Kumar, C.H. Wang, A. Melville, C. Adamo, G. Sheng, Y.H. Chu, J.F. Ihlefeld, R. Erni, C. Ederer, V. Gopalan, L.Q. Chen, D.G. Schlom, N.A. Spaldin, L.W. Martin, R. Ramesh, Science **326**, 977 (2009)
9. Y.Y. Zang, D. Xie, X. Wu, Y. Chen, Y.X. Lin, M.H. Li, H. Tian, X. Li, Z. Li, H.W. Zhu, T.L. Ren, D. Plant, Appl. Phys. Lett. **99**, 132904 (2011)
10. M.M. Kumar, V.R. Palkar, K. Srinivas, S.V. Suryanarayana, Appl. Phys. Lett. **76**, 2764 (2000)
11. H. Uchida, R. Ueno, H. Funakubo, S. Koda. J. Appl. Phys. **100**, 014106 (2006)
12. W. Gao, W.Y. Xing, Q. Yun, C. J. Y Chen, H. Nie, S.F Zhao, J. Mater. Sci. Mater. Electron. **26**, 2127 (2015)
13. T. Kawae, Y. Terauchi, H. Tsuda, M. Kumeda, A. Morimoto, Appl. Phys. Lett. **95**, 112904 (2009)
14. X.B. Xie, S.J. Yang, F.Q. Zhang, S.H. Fan, Q.D. Che, C.J. Wang, X.D. Guo, L.P. Zhang, J. Mater. Sci. Mater. Electron. **26**, 10095 (2015)
15. S.K. Singh, H. Ishiwara, K. Maruyama, Appl. Phys. Lett. **88**, 262908 (2006)
16. W.W. Mao, X.F. Wang, L. Chu, Y.Y. Zhu, Q. Wang, J. Zhang, J.P. Yang, X.A. Li, W. Huang, Phys. Chem. Chem. Phys. **18**, 6399 (2016)
17. C.F. Chung, J.P. Lin, J.M. Wu, Appl. Phys. Lett. **88**, 242909 (2006)
18. V.R. Palkar, J. John, R. Pinto, Appl. Phys. Lett. **80**, 1628 (2002)
19. K.T. Kang, M.H. Lim, H.G. Kim, Y. Choi, H.L. Tuller, I.D. Kim, J.M. Hong, Appl. Phys. Lett. **87**, 242908 (2005)
20. M. Lampert, Phys. Rev. **103**, 1648 (1956)
21. Z. Zhong, H. Ishiwara, Appl. Phys. Lett. **95**, 112902 (2009)
22. K.A. Müller, W. Berlinger, Phys. Rev. B **34**, 6130 (1986)
23. Y. Lin, C. Andrews, H.A. Sodano, J. Appl. Phys. **108**, 064108 (2010)
24. O.G. Vendik, Ferroelectrics **12**, 85 (1976)
25. B. Yu, M. Li, J. Liu, D. Guo, L. Pei, X. Zhao, J. Phys. D Appl. Phys. **41**, 065003 (2008)
26. J. Tauc, Amorphous and Liquid Semiconductors (Plenum Press, New York, 1974), p. 171
27. A. Azam, A. Jawad, A.S. Ahmed, M. Chaman, A.H. Naqvi, J. Alloys Compd. **509**, 2909 (2011)
28. G. L. Song, H. X. Zhang, T. X. Wang, H. G. Yang, F. G. Chang, J. Magn. Magn. Mater **324**, 2121 (2012)
29. S.V. Kiselev, R.P. Ozerov, S. G., Zhdanov. Sov. Phys. Dokl **7**, 742 (1963)
30. Y.H. Lin, Q. Jiang, Y. Wang, C.W. Nan, Appl. Phys. Lett. **90**, 172507 (2007)
31. W.W. Mao, X.F. Wang, Y.M. Han, X.A. Li, Y.T. Li, Y.F. Wang, Y.W. Ma, X.M. Feng, T. Yang, J.P. Yang, W. Huang, S. J. Alloys. Compd. **584**, 520 (2014)